A model of near-sea ice phytoplankton blooms

C. W. Lester,[1,*] T. J. W. Wagner,[2] and Dylan E. McNamara[3]

[1] *Earth and Climate Sciences, Duke University*
[2] *Atmospheric and Oceanic Sciences, University of Wisconsin Madison*
[3] *Physics and Physical Oceanography, University of North Carolina Wilmington*

Author Contributions: All authors conceived of the study idea and developed the methodology. CWL carried out the analysis and wrote the first draft with input from TJWW. All authors contributed to revisions and the final manuscript.

SCIENTIFIC SIGNIFICANCE STATEMENT

Arctic spring blooms of phytoplankton mark the annual emergence of the region's ecosystem from winter dormancy. Satellite observations show that these blooms have increased in size and magnitude in recent years. While this may be expected to be a result of generally warmer conditions, it has been found that near-ice blooms are spatially correlated with cold and fresh surface water signatures from sea ice melt over hundreds of kilometers. This study develops an idealized model that describes how the environmental impact of meltwater may control the spread of phytoplankton spring blooms in the region. The results support the idea that melt-induced stratification of the surface ocean is a dominant driver of recent changes in near-ice bloom characteristics in the Arctic. This furthermore implies that future changes in sea ice cover under continued Arctic warming will have important consequences for the timing and spread of such blooms.

DATA AVAILABILITY STATEMENT

Model code, data, and metadata will be made available in the Dryad data repository.

ABSTRACT

Phytoplankton spring blooms in the Arctic have increased in magnitude and extent over the past two decades, particularly in open waters near the sea ice edge. We develop an idealized model of phytoplankton dynamics that takes into account the role of sea ice meltwater flux and its impact on surface mixed layer depth. Our results suggest a characteristic peak in phytoplankton concentration at around 100 km from the ice edge, in good agreement with satellite observations. This spatial scale emerges from a balance of exponential growth near the ice edge, horizontal advection, and increased decay with distance from the ice as the mixed layer deepens. Observations and data further agree in that meltwater impacts plankton concentrations up to 1000 km from the ice edge. These results suggest that reduced meltwater input under future sea ice retreat may suppress spring phytoplankton blooms in the region.

Keywords: Phytoplankton Blooms, Sea Ice Edge, Arctic Ocean

* Corresponding author contact: conner.lester@duke.edu

I. INTRODUCTION

Phytoplankton blooms occur near the ocean surface along many coastlines around the world. These blooms fuel their local ecosystems and provide sinks for atmospheric carbon (Behrenfeld and Boss 2014; Leu *et al.* 2015; Wassmann and Reigstad 2011). It is less typical for such blooms to be found far from land in open ocean environments. Exceptions to this are observed in the Arctic and Southern Oceans near the edges of sea ice where large open ocean phytoplankton blooms are commonplace (Arrigo and Van Dijken 2003; Behrenfeld *et al.* 2017; Matrai *et al.* 2013; Moreau *et al.* 2019; Zhao *et al.* 2022). A prominent region with such blooms is Fram Strait, between Greenland and the Svalbard Archipelago, which experiences annual spring bursts of large phytoplankton populations near the sea ice edge boundary (Cherkasheva *et al.* 2014; Mayot *et al.* 2020). These ice edge blooms are unique in that they are spatially correlated with the presence of relatively cold and fresh sea ice meltwater, which is suggested to be a key driver in bloom development (Castagno *et al.* 2023; Lester *et al.* 2021; Mayot *et al.* 2020). Over the past two decades, the Fram Strait region has seen an increase in phytoplankton bloom intensities (Lewis *et al.* 2020; Nöthig *et al.* 2015), and these changes have been linked to increased freshwater flux from sea ice melt (Castagno *et al.* 2023).

In this study we focus on the biophysical dynamics of springtime phytoplankton blooms that occur in open water near the sea ice edge. We expand on the idealized model of ice edge blooms of Lester *et al.* (2021). This previous work predicts the existence of a characteristic "bloom curve", which describes the distribution of phytoplankton with distance from the sea ice edge as a function of the distribution of meltwater. Here, we show how this curve emerges from a decade of satellite measurements of near-surface chlorophyll *a* in Fram Strait. We refine the original model by explicitly representing changes in mixed layer depth, and constrain model parameters using satellite observations of chlorophyll *a*, sea surface salinity, and sea ice concentration. We argue that a key control on spring blooms—surface stratification and associated mixed layer depth—is observable through sea surface salinity perturbations from sea ice meltwater near the ice edge. Our results suggest that ice edge phytoplankton bloom dynamics can be described, to leading order, by (i) exponential growth at the ice edge via photosynthesis in a shallow mixed layer that is stratified by sea ice meltwater and (ii) decay of the bloom signal as vertical mixing causes the surface mixed layer to deepen which reduces exposure to sunlight and thereby growth. This simplified picture of complex ice-edge bloom dynamics presents a step toward predicting how annual ice edge blooms may evolve in the presence of climate change and particularly under continued sea ice retreat. Notably, this perspective also suggests the cessation of large open ocean blooms in the region if/when Fram Strait becomes sea ice-free.

II. AN IDEALIZED MODEL OF ICE-EDGE BLOOM DYNAMICS

The dynamics of phytoplankton blooms near the sea ice edge are highly complex and governed by numerous factors, including water temperature, sunlight intensity, nutrient type and availability, fluid stratification and transport, predation, and more (e.g., Behrenfeld and Boss 2014). Our aim is to gain an understanding of specific key processes

by applying several simplifying assumptions, thereby reducing the complexity of the system and making it conceptually and mathematically tractable.

We consider the near-surface phytoplankton concentration $P(\boldsymbol{x}, t)$, averaged over the mixed layer depth, $D(\boldsymbol{x}, t)$, with coordinates $\boldsymbol{x} = (x, y)$ where x is perpendicular and y is parallel to the ice edge orientation (see Appendix A for details). We assume that P evolves to leading order with sunlight-dependent growth and losses from mortality and sinking. Phytoplankton are treated as biological tracers that passively move with the local currents. Within the mixed layer D we assume that such tracers as P, temperature, and salinity are well mixed and approximately homogeneous. Below the mixed layer, phytoplankton concentration decreases rapidly and we take $P \to 0$ for depths greater than D. We generally express the evolution of $P(\boldsymbol{x}, t)$ as

$$\partial_t P + \boldsymbol{u} \cdot \boldsymbol{\nabla} P = \Gamma(P, D)P, \tag{1}$$

where ∂_t is the first time derivative, $\boldsymbol{u}(\boldsymbol{x}, t)$ is the horizontal velocity field and Γ is the depth averaged net growth rate. The second term on the left hand side describes turbulent horizontal mixing of P, following Birch *et al.* (2007).

We eschew the complexities of how fluctuating light environments impact phytoplankton growth (Köhler *et al.* 2018) by taking the growth of $P(\boldsymbol{x}, t)$ in a well mixed layer as approximately "light-limited". This entails that phytoplankton photosynthesize and multiply in proportion to the average light intensity available throughout the mixed layer. And thus growth is reduced when the biomass in the mixed layer increases sufficiently to cause the attenuation of light in the phytoplankton cloud, providing a self-regulating and stabilizing feedback (see Appendix C) (Huisman 1999; Lorenzen 1972). We write the total net growth as

$$\Gamma(P, D) = \gamma I(P, D) - r - \frac{w_P}{D} - \frac{w(D)}{D}, \tag{2}$$

where γ is an effective growth rate determined by sunlight intensity at the surface and $I(P, D)$ is the depth averaged light intensity (normalized by the surface light intensity) which decreases with P and D, r is the effective mortality/respiration rate, w_P is the sinking rate, and the final term is the dilution rate due to the rate of change of the mixed layer depth $w(D)$ (see schematic in Appendix Figure 4)

A notable simplification that these models share is that predation is not explicitly represented. Grazing by zooplankton is highly variable and complex, and for simplicity we take predation to be small relative to the other decay terms during these spring blooms. Beside simplicity, our choice is motivated by the argument that most grazing in the region occurs after peak-bloom conditions (Norrbin *et al.* 2009) and that, for example, *Calanus glacialis* nauplii abundance reaches its maximum later in the season in July–August (Søreide *et al.* 2010). Finally, we assume that the growth rate Γ is not inhibited by nutrient limitations within the mixed layer for the early spring blooms that we are primarily interested in.

Sea ice meltwater stratifies the upper water column, effectively reducing the mixed layer depth and allowing phytoplankton to stay near the sunbathed surface and multiply. At the ice edge, sea ice meltwater is most concentrated

(Castagno *et al.* 2023) and the surface is highly stratified with shallow mixed layer depth $D_0 = D(x = 0)$ (von Appen *et al.* 2021; Peralta-Ferriz and Woodgate 2015). Away from the ice edge the meltwater mixes with the saltier ambient ocean water and the stratification is weakened, leading to an increase in $D(\boldsymbol{x}, t)$. In the far-field open ocean the plankton concentration approaches a background steady state concentration $P_\infty \sim 1/D_\infty$, set by the open ocean mixed layer depth D_∞ (Appendix D)—a relationship predicted in previous models and seen in observations (Huisman 1999; Smith Jr and Jones 2015; Talling 1957). These dynamics for $P(\boldsymbol{x}, t)$ suggest that the observed surface plankton concentrations are the result of rapid growth as low plankton concentrations are advected from the sea ice edge into open waters, and then a decay far from the ice edge from reduced light availability, death, sinking, and dilution as the mixed layer depth increases with the loss of meltwater stratification (Figure 1).

We apply a simplified treatment of the evolution of the mixed layer depth $D(\boldsymbol{x}, t)$ as a fluid boundary problem that can be described using the material derivative such that

$$\partial_t D + \boldsymbol{u} \cdot \boldsymbol{\nabla} D = w(D), \tag{3}$$

where $w(D)$ is the average rate of change of $D(\boldsymbol{x}, t)$. Equation (3) therefore describes the rate at which the mixed layer depth evolves from D_0 at the ice edge towards D_∞ through weakening of meltwater stratification and vertical mixing.

As pointed out in Lester *et al.* (2021), on individual bloom time and spatial scales it is difficult to establish a characteristic spatial bloom curve for $P(\boldsymbol{x})$, due to high spatial heterogeneity in the presence of turbulent mixing, $\boldsymbol{u}(\boldsymbol{x}, t)$. However, when averaged over a sufficiently large set of blooms, or annual blooming seasons, the heterogeneity is smoothed and clear spatial patterns emerge, as shown below.

For a given spring month we approximate the system averaged along the ice edge to be in quasi-steady state, varying slowly over the monthly time scale T_M (Figure 1)—much slower than bloom time scales $T_B \sim \gamma^{-1}$ of order days, such that $T_B \ll T_M$. For a given month, we thus consider small fluctuations about the mean phytoplankton concentration $P(\boldsymbol{x}, t) = \overline{P}(x) + P'(\boldsymbol{x}, t)$, mixed layer depth $D(\boldsymbol{x}, t) = \overline{D}(x) + D'(\boldsymbol{x}, t)$ and horizontal flow $\boldsymbol{u}(\boldsymbol{x}, t) = \overline{\boldsymbol{u}}(x) + \boldsymbol{u}'(\boldsymbol{x}, t)$ in Equations (1) and (3). Quantities $\overline{P}$, $\overline{D}$ and $\overline{\boldsymbol{u}} \equiv U\hat{\boldsymbol{x}}$ are averaged along the ice edge, y, and over a given month. To a first approximation, the average dynamics of Equations (1) and (3) reduce to

$$U\partial_x \overline{P} \simeq \Gamma(\overline{P}, \overline{D})\overline{P} \quad \text{and} \quad U\partial_x \overline{D} \simeq w(\overline{D}). \tag{4}$$

We have assumed advection effects from average flow velocity U are larger than diffusive mixing (Appendix B). From here on, we consider only the monthly-averaged fields, and will drop the overline for clarity of presentation.

Near the ice edge, the mean phytoplankton concentration undergoes exponential growth as

$$P(x) \sim P_0 \exp(x/L_P), \tag{5}$$

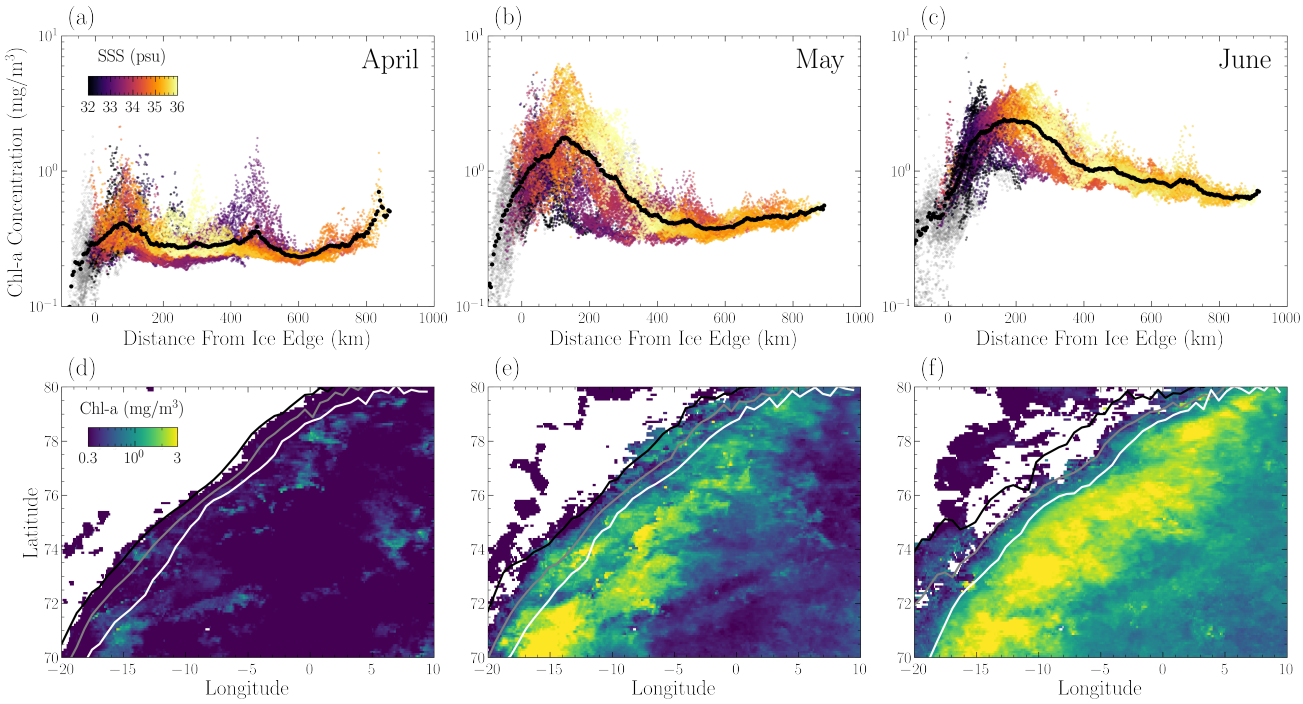

FIG. 1. Chl-a concentrations for (a) April, (b) May, and (c) June, averaged over the years 2011-2019. Concentrations are composites of MODIS Aqua and Terra and VIIRS-SNPP output (see Appendix F). Top row panels (a,b,c) show log-scale chl-a vs distance from sea ice edge where data points are raw data from maps (d,e,f), respectively, and are colored by associated SSS values (see Figure 2). Grey points are chl-a values without an associated SSS value. Solid black points are binned averages. Bottom row panels (d,e,f) show chl-a concentration maps of Fram Strait. White regions indicate missing chl-a data due to presence of sea ice. Lines show the average ice edge location at 75% (black), 50% (grey) and 15% (white) sea ice concentration for each month from the NASA Team algorithm (see Appendix F). For panels (a,b,c) we use sea ice concentration of 50% to define the ice edge $x = 0$.

where $L_P = U/\Gamma(P_0, D_0)$ is a characteristic length scale that balances the horizontal transport with the plankton growth rate. Far from the ice edge the concentration decays towards $P(x) \to P_\infty \sim 1/D_\infty$, suggesting that the surface phytoplankton concentration is maximized at some nontrivial distance away from the ice edge—defining the characteristic bloom curve $P(x)$ (Lester *et al.* 2021).

III. RESULTS AND DISCUSSION

To observe the spatial patterns of ice-edge blooms we analyze monthly averages of surface chl-a concentrations in Fram Strait from 2011-2019 (see Appendix F). As seen in Figure 1 these monthly averages reveal patterns of steep chl-a increase near the ice edge and more gradual decay towards the open ocean, supporting the general bloom curve prediction from Lester *et al.* (2021). We next consider whether the model of Equations (4) can capture this feature.

In order to constrain our model using observations, we use SSS as a proxy of mixed layer depth, motivated by the observed dominance of near-surface stratification in determining the variability of mixed layer depth (Peralta-Ferriz and Woodgate 2015). Recent advances in satellite technology mean that SSS in the Arctic can be observed with good spatial and temporal cover by satellites, while direct measurements of mixed layer depths are much more sporadic.

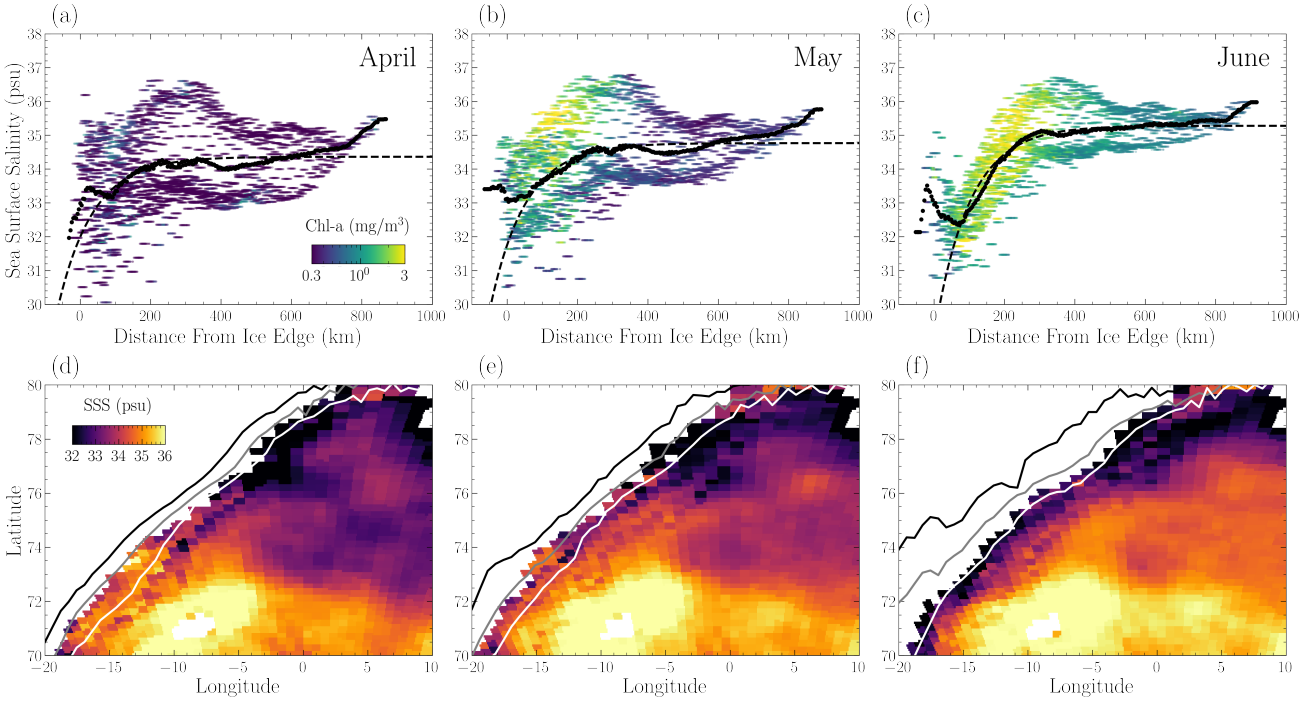

FIG. 2. Sea surface salinity (SSS) for April, May and June averaged over the years 2011-2019 (see Appendix F). Top row panels (a,b,c) show SSS vs distance from sea ice edge where data points are raw data from maps (d,e,f), respectively, and are colored by associated chl-a values (see Figure 1). Solid black points are binned averages and dashed lines are fitted e-folding curves with saturation length scale $L_{\rm SSS} = 100$ km. Fits for $L_{\rm SSS}$ vary little between months and are thus held constant at 100 km for simplicity. Bottom row panels (d,e,f) show SSS maps of Fram Strait. As in Figure 1, white regions indicate missing data due to presence of sea ice and lines show the average ice edge location at SIC = 75% (black), 50% (grey) and 15% (white). Again, panels (a,b,c) use SIC = 50% to define $x = 0$. We note that the concentrated region of high SSS $\gtrsim 35$ psu is around the island of Jan Mayen. Excluding data near Jan Mayen does not significantly change the results—it primarily reduces the average SSS(x) in panels (a,b,c) by a constant offset, and it does not notably alter the chl-a(x) distributions of Figure 1.

Figure 2 shows spatial patterns of SSS for spring months averaged over the study period 2011-2019 (Appendix F), exhibiting patterns of low SSS near the ice edge, suggesting a shallow mixed layer, and high values of SSS far from the ice edge, suggesting a larger mixed layer. When averaged along the sea ice edge the pattern is accentuated, revealing how the salinity relaxes from a lower value near the ice edge, $\mathrm{SSS}_0 \sim 30 - 33$ psu, to an open ocean value, $\mathrm{SSS}_\infty \sim 35$ psu, at a rate determined by the saturation length scale $L_{\rm SSS}$ (Figure 2).

If D is primarily a function of SSS, then for small perturbations to SSS_∞ we can write $D_\infty - D \propto \mathrm{SSS}_\infty - \mathrm{SSS}$ and thus $\partial_x D \propto \partial_x \mathrm{SSS}$. We therefore model the mixed layer evolution, informed by the observed SSS fields of Figure 2, as

$$\partial_x D \simeq \frac{D}{L_D}\left(1 - \frac{D}{D_\infty}\right), \tag{6}$$

where $L_D \simeq L_{\rm SSS}$. This representation of $D(x)$ allows for a closed solution to the average phytoplankton distribution $P(x)$ which is a function of (i) the fairly well constrained parameters I, r, and w_P, (ii) several other in principle measurable parameters such as phytoplankton concentrations at the ice edge P_0 and in the open ocean P_∞, (iii) the length scales L_P and L_D and (iv) the mixed layer depths D_0 and D_∞. Observations of mean chl-a(x) in Figure 1

allow us to infer P_0 and P_∞ if we assume $P \propto$ chl-a. The growth length scale L_P can be estimated from the rate of exponential growth near the ice edge (Figures 1, 3). From observations of SSS(x) in Figure 2 we can approximate the length scale $L_D \simeq L_{\mathrm{SSS}}$.

Due to lack of in-situ measurements of surface insolation and the complexity of phytoplankton growth under fluctuating light conditions (Köhler *et al.* 2018) it is challenging to directly measure the light dependent growth rate scale γ. We similarly do not have direct measurements of D_0 or D_∞. However, we are able to estimate the value of γ from measurements of L_P and similarly we can approximate the mixed layer depth D_∞ from the dynamics that lead to P_∞ (see Appendix D for details). Thus our model only uses a single unconstrained fitting parameter, D_0. For the three months under consideration here, we find best fits between the observed chl-a distribution and the theoretical bloom curves when $D_0 = 31$ m in April, $D_0 = 15$ m in May, and $D_0 = 7.5$ m in June. These values agree well with measurements in the region (Peralta-Ferriz and Woodgate 2015). The relative importance of the individual terms in Equation (2) for these parameter values is shown in Appendix Figure 5.

From the monthly values of chl-a(x) averaged over the years 2011-2019 (Figures 1, 3; Appendix F) we are able to clearly describe not only the start of the spring phytoplankton bloom season in Fram Strait, but also the spatial bloom curve as a function of distance to the ice edge for each month. Namely, close to the sea ice edge we observe exponential growth trends as predicted above (Eq. 5) with length scale L_P varying around ~ 100 km. The approximated growth rate γ is found to be around 0.5 day^{-1}—consistent with measurements (Eppley 1972; Huisman 1999; Smith Jr *et al.* 1987). Additionally, the estimated γ values increase with clear-sky insolation in Fram Strait from April to June (Figure 3f, inset), supporting our assumption that blooms are in a light-limited regime.

The observations are consistent with the dynamics proposed in this model: when phytoplankton are initially advected from the ice edge into open water, they grow quickly within a shallow mixed layer that is stratified by sea ice meltwater. As they are further advected and grow the meltwater begins to mix with the ocean waters. This elevates SSS and reduces the capacity of phytoplankton growth as the mixed layer deepens (Huisman 1999). In between the extremes of exponential phytoplankton growth at the ice edge, marked by small chl-a and small SSS near $x = 0$, and bloom decay far from the ice edge, marked by small chl-a and large open-ocean SSS as $x \to \infty$, we observe the chl-a maximum. This is located at an intermediate SSS value (~ 34 psu) at a characteristic distance (~ 100 km) from the ice edge (Figure 3).

The model predicts that the bloom magnitude $P_{\max} \sim \gamma/D_0 \sim \gamma M_0$ increases with the growth rate scale γ as well as the sea ice melt rate at the ice edge $M_0 \sim 1/D_0$ (see Appendix E). This is of particular relevance because both of these parameters are subject to vary under climate change: γ will likely increase with surface temperatures (Eppley 1972) and be impacted by changes in cloud cover; the melt rate M_0 also stands to increase as surface temperatures increase under global warming (at least transiently), exacerbated in this region by Arctic Amplification (England *et al.* 2021). This combination of factors suggests that in the near-term ice-edge phytoplankton blooms will continue to increase in magnitude and appear earlier in the spring. Importantly however, a retreat of sea ice in the region would signify reduced blooming. If Fram Strait ever becomes sea ice free in the spring months, this model predicts

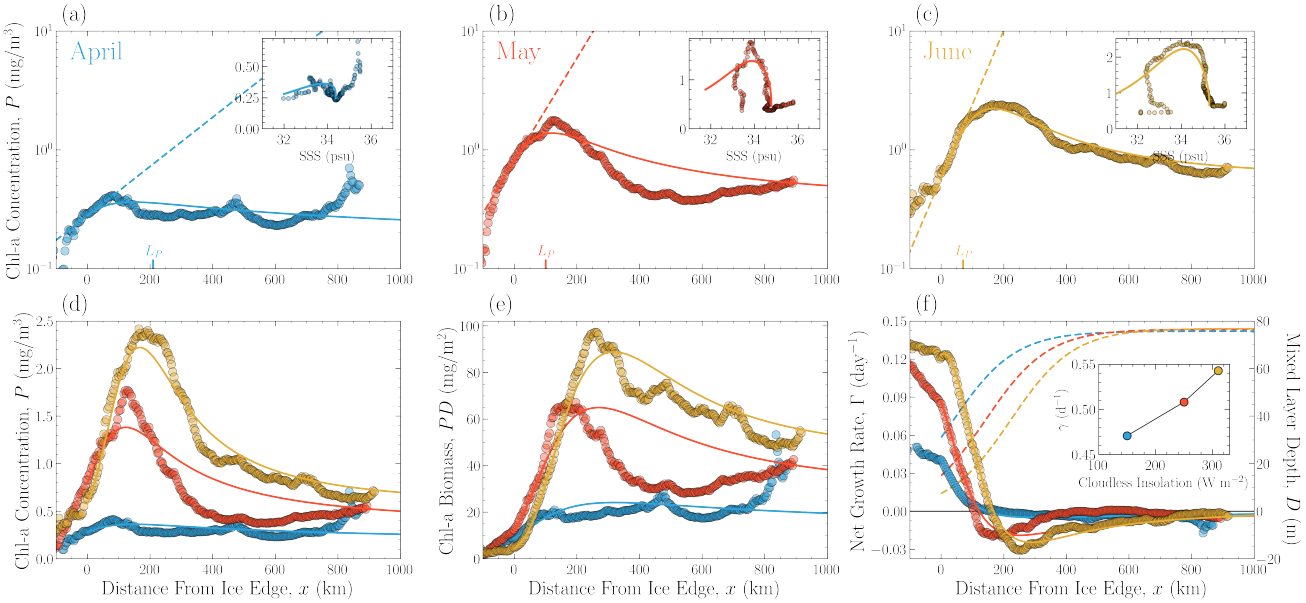

FIG. 3. Model-observation comparison for P and chl-a. Top row panels (a,b,c) show chl-a concentration vs distance from the mean ice edge. Filled markers correspond to the mean values (black dots) from Figure 1. Dashed lines are exponential growth functions (Eq. 5) giving the length scale $L_P = U/\Gamma(P_0, D_0)$—marked on the horizontal axis of each plot. Solid lines show solutions of $P(x)$ for Equations (4) and (6) using $L_D = 100$ km and fit parameter $D_0 = (31, 15, 7.5)$ m for April, May and June, respectively. Insets show binned chl-a concentrations vs binned SSS values from Figure 2 (markers). Lines are the $P(x)$ solutions of the larger panels vs the fitted SSS(x) from the dashed lines in Figure 2. Panel (d) overlays the information from panels a,b,c, now on a linear scale. Panel (e) shows biomass concentrations $P(x)D(x)$ and chl-a(x)$D(x)$ using the modeled mixed layer depths $D(x)$. Panel (f) shows the dependence of growth rate $\Gamma(P, D)$ (Eq. 2) on distance from the ice edge. Markers are computed from Equation (2) using chl-a(x) distributions and model parameters from predictions in (a,b,c). We note that growth rates Γ measured using gradients from the data Δchl-a/Δx (i.e., Eq. 4) are highly variable but shows similar trends. The dashed lines in (f) shows the modeled mixed layer depths $D(x)$ (right axis) and the inset shows an estimation of the growth rate scale γ (Appendix Eq. D1) plotted against observed clear-sky insolation in Fram Strait for each month (insolation data from Castagno *et al.* (2023)).

the complete cessation of these characteristic bloom curves, and the plankton distribution would instead approach a uniform value P_∞.

Lastly, we note an important consequence of considering the depth-averaged plankton concentration $P(x)$ as a property of the mixed layer depth: In this framework, the predicted total biomass is given by $B(x) = P(x)D(x)$. The biomass distribution B is less strongly dependent on x than P is, since a part of the x-dependence is due to the compression/dilution that results from changes in D. As a result, $P_{\max} \simeq 4P_\infty$, while the peak in biomass $B_{\max}$ is only roughly twice that of B_∞ (Figure 3e). In other words, in this model framework approximately half of the near-surface plankton peak near the ice edge is due to increased growth and the other half is due to the plankton being confined more closely to the surface. This also suggests that at least part of the observed recent increases in near-surface chl-a in the Fram Strait region may be due to the plankton being more closely confined to the surface, rather than purely an increase in overall biomass.

IV. CONCLUSION

We have presented an idealized modeling framework to understand the distribution of phytoplankton during the spring blooming period as influenced by sea ice melt. By accounting for the impacts of light-limited growth, meltwater-induced stratification of the mixed layer, and advection we reproduce the observed characteristic spatial distributions. Our results support the idea that freshwater flux from sea ice melt plays a crucial role in determining the magnitude and spread of near-ice phytoplankton blooms. This is largely because the increased surface stratification allows the plankton to spend more time exposed to sunlight, allowing for greater growth rates. Our findings have implications for the future evolution of Arctic spring blooms as the pattern of sea ice meltwater release is rapidly changing under global and Arctic-amplified warming. Our results motivate more detailed studies that account for other important processes and that carry greater spatial fidelity by resolving horizontal and vertical variability.

von Appen, W.-J., A. M. Waite, M. Bergmann, C. Bienhold, O. Boebel, A. Bracher, B. Cisewski, J. Hagemann, M. Hoppema, M. H. Iversen, *et al.* (2021), Nature Communications **12** (1), 7309.

Arrigo, K. R., and G. L. Van Dijken (2003), Journal of Geophysical Research: Oceans **108**, C8.

Behrenfeld, M. J., and E. S. Boss (2014), Annual Review of Marine Science **6** (1), 167.

Behrenfeld, M. J., Y. Hu, R. T. O'Malley, E. S. Boss, C. A. Hostetler, D. A. Siegel, J. L. Sarmiento, J. Schulien, J. W. Hair, X. Lu, *et al.* (2017), Nature Geoscience **10** (2), 118.

Beszczynska-Möller, A., E. Fahrbach, U. Schauer, and E. Hansen (2012), ICES Journal of Marine Science **69** (5), 852.

Birch, D. A., Y.-K. Tsang, and W. R. Young (2007), Physical Review E **75** (6), 066304.

Castagno, A. P., T. J. W. Wagner, M. R. Cape, C. W. Lester, E. Bailey, C. Alves-de Souza, R. A. York, and A. H. Fleming (2023), Global Change Biology **29** (17), 5087, https://onlinelibrary.wiley.com/doi/pdf/10.1111/gcb.16815.

Cavalieri, D. J., C. Parkinson, P. Gloersen, and H. J. Zwally (1996), "Sea ice concentrations from Nimbus-7 SMMR and DMSP SSM/I-SSMIS passive microwave data,".

Cherkasheva, A., A. Bracher, C. Melsheimer, C. Köberle, R. Gerdes, E.-M. Nöthig, E. Bauerfeind, and A. Boetius (2014), Journal of Marine Systems **132**, 196.

Eilers, P., and J. Peeters (1988), Ecological modelling **42** (3-4), 199.

England, M. R., I. Eisenman, N. J. Lutsko, and T. J. Wagner (2021), Geophysical Research Letters **48** (15), e2021GL094086.

Eppley, R. W. (1972), Fish. bull **70** (4), 1063.

Hintz, N. H., B. Schulze, A. Wacker, and M. Striebel (2022), Ecology and Evolution **12** (3), e8753.

Huisman, J. (1999), Ecology **80** (1), 202.

Köhler, J., L. Wang, A. Guislain, and T. Shatwell (2018), Limnology and Oceanography **63** (3), 1156.

Lester, C. W., T. J. W. Wagner, D. E. McNamara, and M. R. Cape (2021), Geophysical Research Letters **48** (2), e2020GL091758.

Leu, E., C. J. Mundy, P. Assmy, K. Campbell, T. M. Gabrielsen, M. Gosselin, T. Juul-Pedersen, and R. Gradinger (2015), Progress in Oceanography **139**, 151.

Lewis, K., G. Van Dijken, and K. R. Arrigo (2020), Science **369** (6500), 198.

Lorenzen, C. J. (1972), ICES Journal of Marine Science **34** (2), 262.

Matrai, P., E. Olson, S. Suttles, V. Hill, L. Codispoti, B. Light, and M. Steele (2013), Progress in Oceanography **110**, 93.

Mayot, N., P. Matrai, A. Arjona, S. Bélanger, C. Marchese, T. Jaegler, M. Ardyna, and M. Steele (2020), Journal of Geophysical Research: Oceans **125** (3), e2019JC015799.

Moreau, S., D. Lannuzel, J. Janssens, M. Arroyo, M. Corkill, E. Cougnon, C. Genovese, B. Legresy, A. Lenton, V. Puigcorbe, *et al.* (2019), Journal of Geophysical Research: Oceans **124** (5), 2943.

NASA Ocean Biology Processing Group, GSFC, (2017), doi:10.5067/NPP/VIIRS/L3M/CHL/2018.

NASA Ocean Biology Processing Group, GSFC, (2021), doi:10.5067/AQUA/MODIS/L3M/CHL/2021.

NASA Ocean Biology Processing Group, GSFC, (2022), doi:10.5067/TERRA/MODIS/L3M/CHL/2022.

Naselli-Flores, L., T. Zohary, and J. Padisák (2021), Hydrobiologia **848** (1), 7.

Norrbin, F., H. C. Eilertsen, and M. Degerlund (2009), Deep Sea Research Part II: Topical Studies in Oceanography **56** (21-22), 1945.

Nöthig, E.-M., A. Bracher, A. Engel, K. Metfies, B. Niehoff, I. Peeken, E. Bauerfeind, A. Cherkasheva, S. Gäbler-Schwarz, K. Hardge, *et al.* (2015), Polar Research **34** (1), 23349.

Peralta-Ferriz, C., and R. A. Woodgate (2015), Progress in Oceanography **134**, 19.

Sakshaug, E., and D. Slagstad (1991), Polar Research **10** (1), 69.

Sathyendranath, S., R. J. Brewin, C. Brockmann, V. Brotas, B. Calton, A. Chuprin, P. Cipollini, A. B. Couto, J. Dingle, R. Doerffer, *et al.* (2019), Sensors **19** (19), 4285.

Smith Jr, W. O., M. E. Baumann, D. L. Wilson, and L. Aletsee (1987), Journal of Geophysical Research: Oceans **92** (C7), 6777.

Smith Jr, W. O., and R. M. Jones (2015), ICES Journal of Marine Science **72** (6), 1952.

Søreide, J. E., E. V. Leu, J. Berge, M. Graeve, and S. Falk-Petersen (2010), Global change biology **16** (11), 3154.

Supply, A., J. Boutin, J.-L. Vergely, N. Kolodziejczyk, G. Reverdin, N. Reul, and A. Tarasenko (2020), Remote Sensing of Environment **249**, 112027.

Talling, J. (1957), The New Phytologist **56** (2), 133.

Wassmann, P., and M. Reigstad (2011), Oceanography **24** (3), 220.

Zhao, H., A. Matsuoka, M. Manizza, and A. Winter (2022), Journal of Geophysical Research: Oceans , e2021JC018346.

Appendix A: Phytoplankton Distribution in a Mixed Layer

We consider the evolution of phytoplankton concentration $p(z, \boldsymbol{x}, t)$ (mass of plankton per unit volume) as a passive tracer, the dynamics of which are governed by

$$\mathrm{D}_t p = \widetilde{\Gamma} p, \tag{A1}$$

where $\widetilde{\Gamma}$ is the net growth rate which is generally composed of phytoplankton production from light and nutrient uptake and losses from mortality, respiration, sinking, and predation.

Here, we are interested in the evolution of $p(z, \boldsymbol{x}, t)$ as averaged over the surface mixed layer with depth boundary $D(\boldsymbol{x}, t)$. We take the phytoplankton to be well mixed within the surface mixed layer, such that $p(z, \boldsymbol{x}, t) = P(\boldsymbol{x}, t) + p'(z, \boldsymbol{x}, t)$, where $P(\boldsymbol{x}, t)$ is the depth averaged plankton concentration and $p'(z, \boldsymbol{x}, t)$ are considered small perturbations from the average. Similarly, the horizontal flow field is regarded as the depth averaged flow $\boldsymbol{u}(\boldsymbol{x}, t)$ plus fluctuations $\boldsymbol{u}'(z, \boldsymbol{x}, t)$. Averaging over the fast fluctuation time scales and over depth $D(\boldsymbol{x}, t)$, Equation (A1) reduces to Equation (1).

Appendix B: Quasi-Steady Dynamics

To facilitate direct comparisons to satellite data, we consider the quasi-steady state dynamics (see main text Section II). The phytoplankton evolution averaged along the ice edge and over monthly time scales can then be approximated as

$$U\partial_x \overline{P} \simeq \Gamma(\overline{P}, \overline{D})P + \kappa \partial_{xx}^2 \overline{P}$$

where κ is the turbulent diffusivity—whose main effect in this framework is to simply smooth $\overline{P}(x)$. We can define the Péclet number $\mathrm{Pe} = |\Gamma|^{-1}U^2/\kappa$, where $|\Gamma|^{-1}U$ is the characteristic bloom length scale given by the ratio of the advection scale U and growth rate $|\Gamma|$. Here, κ/U is the characteristic turbulent length scale. For $\mathrm{Pe} \gg 1$ turbulent diffusion becomes negligible and the system is governed by mean advection. For a typical growth rate scale $|\Gamma| \sim 0.1$ day^{-1} and $U \sim 0.1$ m/s, the bloom length is of order $\sim$100 km (Figure 1). Ocean diffusivity scales are of order 100 m^2/s suggesting turbulent lengths of order kilometers. Thus we assume a regime where $\mathrm{Pe} \gg 1$ and are left with the time averaged model in the main text (Equation 4). We omit the overlines below for clarity.

Appendix C: Growth Rate

We consider a leading-order representation of early spring blooms and consider growth to be mainly determined by sunlight availability. We thus assume that the growth rate Γ is dependent on the light intensity $\widetilde{I}(p, z) \simeq \widetilde{I}(P, z)$

but not inhibited by nutrient limitations within the mixed layer for the early spring blooms that we are primarily interested in.

The light intensity (normalized by the surface value) at depth z is given by the Beer-Lambert Law as

$$\widetilde{I}(P,z) = \exp\left(-\frac{z}{\ell_f} - \frac{P}{\rho_P}\frac{z}{\ell_P}\right) \equiv \exp\left(-\frac{z}{\ell_0}\right),$$

with the characteristic decay length defined by $1/\ell_0 \equiv 1/\ell_f + P/K_B$ where ℓ_f is the fluid light attenuation length and $K_B = \rho_P \ell_P$ is an effective biomass carrying capacity scale set by the average phytoplankton density of a single cell ρ_P and the phytoplankton light attenuation length ℓ_P (Huisman 1999). For light dependent phytoplankton growth, controlled experiments show that the growth rate scales linearly with low light intensity (light-limited regime) relative to a respiration threshold, whereas for large light intensities the growth rate becomes roughly constant (saturated regime) (Eilers and Peeters 1988; Hintz *et al.* 2022). However, under fluctuating light conditions, like in a mixed layer, the saturated regime occurs at much larger light intensities than in constant light conditions (Köhler *et al.* 2018). For this reason and because the depth averaged light intensity varies relatively slowly we approximate the phytoplankton growth-light relationship as linear. Thus we may write the net depth averaged growth rate as

$$\Gamma(P,D) \simeq \gamma I(P,D) - r - w_P/D - w(D)/D,$$

which is the same as Equation (2). Here, γ is the growth rate scale proportional to the light intensity at the surface, $I = (\ell_0/D)(1 - e^{-D/\ell_0})$ is the depth averaged (normalized) light intensity, r is the mortality/respiration rate and w_P is the phytoplankton sinking velocity.

Appendix D: Parameter Estimation

Equations (1)-(3) present a closed model for ice edge phytoplankton growth. We assume the following rough values of experimentally measured parameters used in Figure 3: $\ell_f = 20$ m, $K_B = 50$ mg Chl-a/m^2, $r = 0.1$ day^{-1} and $w_P = 1$ m/day (Eppley 1972; Lorenzen 1972; Naselli-Flores *et al.* 2021; Sakshaug and Slagstad 1991). Additionally, we let $U = 0.1$ m/s which is on the order of typically observed speeds in Fram Strait (Beszczynska-Möller *et al.* 2012). The remaining values to constrain are $P_\infty,\ P_0,\ \gamma,\ D_\infty$ and D_0. $P(x \to \infty) = P_\infty$ and $P(x = 0) = P_0$ are inferred from from chl-a observations in Figure 3 (see Section F below). The growth rate scale γ is in principle given by the surface light intensity. However, predictions of surface light intensity in Fram Strait are often only provided for cloudless skies and the presence of clouds can reduce the light intensity by nearly an order of magnitude (Sakshaug and Slagstad 1991). Here, we choose to measure γ via the exponential growth length scale L_P as defined by

$$L_P^{-1} = \frac{\gamma}{U} I(P_0, D_0) - \frac{r}{U} - \frac{w_P}{U D_0} - L_D^{-1}\left(1 - \frac{D_0}{D_\infty}\right), \tag{D1}$$

where most of the monthly variations in L_P seem to be set by γ (Figure 3). Similarly, information about the open ocean mixed layer depth is (in principle) encapsulated in the dynamics of $P(x)$—specifically in P_∞. Thus D_∞ can be solved for when $\Gamma = 0$ or:

$$\gamma I(P_\infty, D_\infty) - r - \frac{w_P}{D_\infty} = 0. \tag{D2}$$

To a good approximation the open ocean phytoplankton concentration is in this case given by

$$P_\infty \simeq \frac{K_B}{D_\infty}\left(\frac{\gamma}{r + \frac{w_P}{D_\infty}} - \frac{D_\infty}{\ell_f}\right), \tag{D3}$$

showing that the open ocean concentration is set by the biomass capacity K_B relative to the open ocean mixed layer depth D_∞. It also increases with light intensity γ. This also suggests that $D_\infty \lesssim \gamma \ell_f / r$, otherwise the open ocean concentration would vanish.

This leaves one free parameter, the depth of the mixed layer at the ice edge, D_0. This quantity is not readily constrained. We therefore use it as a fitting parameter and compare the fits to observational estimates (von Appen *et al.* 2021; Peralta-Ferriz and Woodgate 2015).

Appendix E: Phytoplankton Maximum

The maximum phytoplankton concentration $P_{\max}$ can be found when $\Gamma = 0$ at critical mixed layer depth $D_* = D(P_{\max})$ as

$$P_{\max} \simeq \frac{K_B}{D_*}\left(\frac{\gamma}{r + \frac{w_P}{D_*} + \frac{U}{L_D}\left(1 - \frac{D_*}{D_\infty}\right)} - \frac{D_*}{\ell_f}\right). \tag{E1}$$

From Figure 3 we see that $P_{\max}$ occurs close to the ice edge such that the critical depth scales as $D_* \propto D_0$ (rather than scaling with D_∞ far from the ice edge). It is found that the mixed layer depth at the ice edge decrease as the sea ice melt rate M_0 (the fresh water flux) increase, $D_0 \sim 1/M_0$ (Castagno *et al.* 2023). Therefore because $P_{\max} \sim 1/D_0$ this suggests that $P_{\max} \sim \gamma K_B M_0$.

Appendix F: Observational Data

The core observations we use to constrain the model above are satellite measurements of chlorophyll *a* (chl-a), sea surface salinity (SSS), and sea ice concentration (SIC).

Near-surface chl-a concentration data for the years 2011–2019 were averaged over the monthly Level 3 products from three sensors: MODIS Aqua (NASA Ocean Biology Processing Group, GSFC 2021), MODIS Terra (NASA Ocean Biology Processing Group, GSFC 2022), and VIIRS-SPNN (NASA Ocean Biology Processing Group, GSFC

2017), all at 9 km resolution. We use these datasets rather than the merged Ocean-Colour Climate Change Initiative (OC-CCI) product (Sathyendranath *et al.* 2019) because OC-CCI features large and seemingly spurious variability right at the ice edge (not shown). These issues are not found in the individual sensor data or when computing the average of the three sensors listed above.

To assess the impact of meltwater on surface salinity we use Version 1 of the monthly Level 3 Soil Moisture and Ocean Salinity (SMOS) Arctic SSS product provided by LOCEAN (Supply *et al.* 2020) at 25 km resolution. This product spans from June 2010 to November 2019 and covers the Arctic region north of 60°N. Since we are interested in the spring bloom period (April–June) we limit our study period to years 2011–2019. To estimate the location of the sea ice edge, we use SIC for Fram Strait spanning the years 2011 to 2019 from SMMR-SSM/I data processed with the NASA Team algorithm (Cavalieri *et al.* 1996) at 25 km resolution.

The focus of this study is how chl-a and SSS vary with distance from the sea ice edge. To compute this dependence, we determine the distance to the sea ice edge (defined as the SIC = 50% contour) for each grid box on all monthly distribution maps. We then calculate the values of chl-a and SSS at each location and bin the data as a function of distance from the ice edge. Finally, we average over the years 2011–2019 to get the decadal-mean monthly curves for April, May, and June as functions of distance from the sea ice edge. The SIC contours for 15%, 50%, and 75% run in approximately straight and parallel lines from the northeast (near Svalbard) to the southwest (see Figure 1). This enables us to consider how chl-a and SSS vary in the direction perpendicular to the ice edge by averaging the data in the direction parallel to the ice edge.

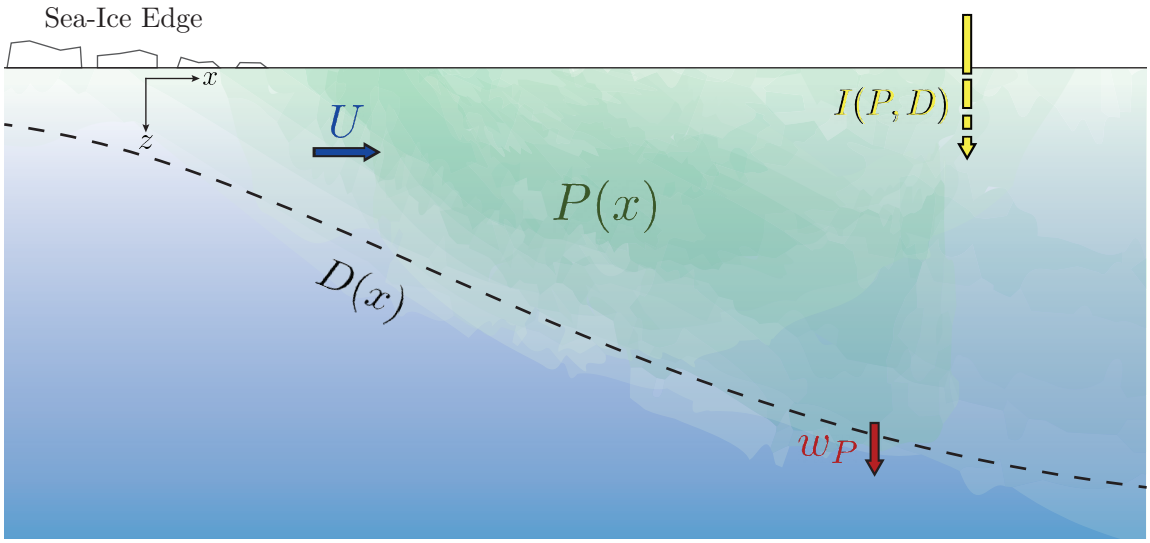

FIG. 4. Schematic of simplified phytoplankton bloom dynamics within a mixed layer stratified by meltwater. Dashed line shows the mixed layer depth $D(x)$ increasing with distance from the ice edge as the sea-ice meltwater mixes increasingly with salty ambient open-ocean waters. The phytoplankton concentration within the mixed layer $P(x)$ is advected from the ice edge at rate U and grows at a rate determined by sunlight intensity averaged over the mixed layer $I(P, D)$. The concentration $P(x)$ decreases from dilution as the mixed layer depth increases $D(x)$, from sinking out of the mixed layer at rate w_P, and from natural mortality/respiration at rate r (not shown).

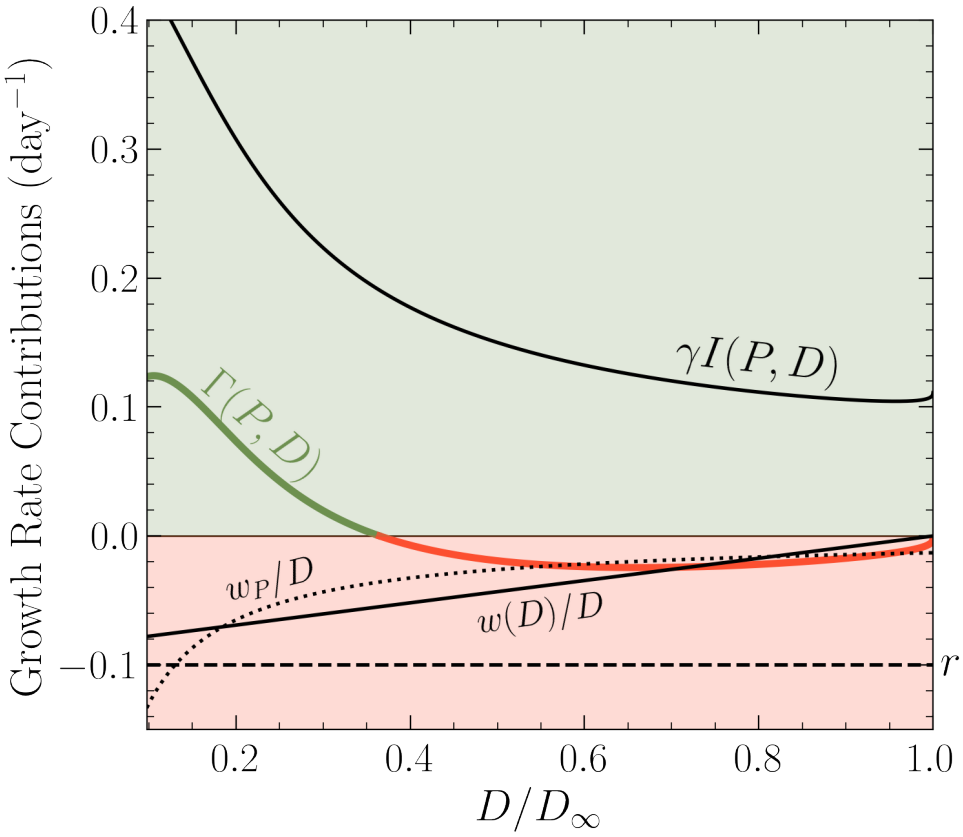

FIG. 5. Depth averaged net growth rate $\Gamma(P, D)$ partitioned by individual contributions as a function of rescaled mixed layer depth D/D_∞. Green region is positive growth and red is negative growth (phytoplankton death/loss and dilution of the average P). Parameters are as used for the month of June in Figure 3. Other months look similar.